

Non-linear and quantum optics of a type II OPO containing a birefringent element

2. Bright entangled beams generation

L. Longchambon, J. Laurat, T. Coudreau^a, and C. Fabre

Laboratoire Kastler Brossel, Case 74, UPMC, 4 place Jussieu, 75252 Paris Cedex 05, France

Received 18 November 2003 / Received in final form 12 February 2004

Published online 23 July 2004 – © EDP Sciences, Società Italiana di Fisica, Springer-Verlag 2004

Abstract. We describe theoretically the quantum properties of a type-II Optical Parametric Oscillator containing a birefringent plate which induces a linear coupling between the orthogonally polarized signal and idler beams and results in phase locking between these two beams. As in a standard OPO, the signal and idler waves show large quantum correlations which can be measured experimentally due to the phase locking between the two beams. We study the influence of the waveplate on the various criteria characterizing quantum correlations. We show in particular that the quantum correlations can be maximized by using optimized quadratures.

PACS. 42.65.Yj Optical parametric oscillators and amplifiers – 42.25.Lc Birefringence – 42.50.Lc Quantum fluctuations, quantum noise, and quantum jumps

1 Introduction

The domain of quantum information with intense light beams is becoming more and more studied as practical applications are developed [1–3]. A large number of experiments rely on so-called EPR beams, that is a pair of fields containing quantum correlations on two different non commuting observables [4]. Several methods have been used to date. One way to generate them is to mix two independent squeezed beams produced by two independent OPOs below threshold [1,5], or by third order non linearity in a fiber [3]. Another configuration consists in using a non degenerate OPO below threshold [6–8]. We propose here a new method where two bright entangled beams are produced directly at the output of a non degenerate OPO pumped above threshold.

Optical Parametric Oscillators are very efficient sources of non classical light [9–14]. In particular, it has been shown experimentally that the intensities of the signal and idler beams exhibit very large quantum correlations [9,11,14]. It is also predicted that the phase of the signal and idler should show quantum anticorrelations [15]. However, the measurement of these phase anticorrelations is not possible in a standard OPO in which frequency degenerate operation occurs only accidentally and is very sensitive to thermal and mechanical drifts. Thus, in practical experiments, the frequencies of the signal and idler beam are different. This implies that the relative phase between the two fields has a rapidly varying component. Furthermore, even if the device is actively

stabilized on the frequency degeneracy working point [16], this relative phase between signal and idler undergoes a diffusion process [17], similarly to the phase of a laser field. In order to be able to measure experimentally these phase anticorrelations, one can use a phase locked OPO: one possible technique proposed in [18] is to use a birefringent plate inserted inside the OPO cavity and making an angle with the axis of the non-linear crystal which leads to self-phase locking. This phenomenon has been studied in detail in [19,20] at the classical level. It is the purpose of this paper to evaluate the influence of the phase locking mechanism on the quantum properties of the system.

The paper is organized as follows. In Section 2, we give the equations describing the quantum fluctuations of the system. We study in Section 3 the noise spectra of the amplitude quadratures difference and phase quadratures sum showing quantum noise reduction, i.e. that these variances are below what would be observed for independent coherent states. In Section 4, various entanglement criteria are discussed, namely EPR correlation properties (Sect. 4.1), inseparability criterion (Sect. 4.2) and teleportation fidelity (Sect. 4.3). Finally, Section 5 is devoted to the case of non-orthogonal quadratures which enable us to increase dramatically the violation of the inseparability criterion.

2 Basic equations

In order to calculate the fluctuations for the signal and idler fields when the OPO is pumped above threshold,

^a e-mail: coudreau@spectro.jussieu.fr

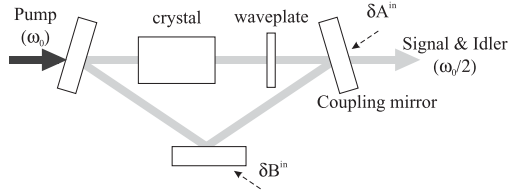


Fig. 1. Ring cavity OPO with the fluctuations corresponding to the fluctuations coming through the input mirror (δA_i^{in}) and the fluctuations due to the losses (δB_i^{in}).

we apply the input-output linearization technique described e.g. in [26]. We first determine the classical stationary solutions of the evolution equations: these solutions are denoted $A_i^{(s)}$ where $i = 0, 1, 2$ corresponds to the pump, signal and idler fields. We then linearize the evolution equations around these stationary values by setting: $A_i = A_i^{(s)} + \delta A_i$, $i = 0, 1, 2$. Introducing the input fluctuations in all the modes, we obtain a set of linear coupled equations for the fluctuations of the different fields. By solving these equations in the Fourier domain, one can calculate the individual noise spectra as well as the correlations between the different quadratures.

Let us recall the system under study which has been discussed in detail in [20]. We consider a $\chi^{(2)}$ medium placed inside a ring optical cavity doubly resonant for signal and idler (Fig. 1). Type-II phase-matching results in orthogonally polarized signal and idler fields. The reflection coefficients for signal and idler are assumed to be equal in module: $r_j = r \exp(i\zeta_j)$, $j = 1, 2$. We assume also that the cavity has a high finesse for these modes so that we can write $r = 1 - \kappa$ with $\kappa \ll 1$; the transmission is thus $t \approx \sqrt{2\kappa}$. Finally, the cavity is characterized by the round-trip losses for the signal and idler waves (crystal absorption, surface scattering...), μ , and we define a generalized reflection coefficient: $r' = r(1 - \mu) \approx 1 - (\mu + \kappa) = 1 - \mu'$.

Let us denote l the crystal length and L the free propagation length inside the cavity. The crystal indices of refraction are n_1 and n_2 respectively for the signal and idler waves. The waveplate is rotated by an angle ρ with respect to the crystal neutral axes. In contrast to [20], we assume here that this angle is small.

The crystal is birefringent and can be characterized by its mean index \bar{n} , birefringence θ and effective nonlinear coupling constant g :

$$\bar{n} = \frac{n_1 + n_2}{2} \quad (1)$$

$$\theta = \frac{\omega_0}{2c}(n_2 - n_1)l \quad (2)$$

$$g = l\chi^{(2)}\sqrt{\frac{\hbar\omega_0\omega_1\omega_2}{2c^3\varepsilon_0n_0n_1n_2}} \quad (3)$$

where $\omega_0/2$ is the common frequency of signal and idler.

The mean round trip phase-shift is $\delta = (\omega_0/2c)(ne + \bar{n}l + L) + \bar{\zeta}$ where $\bar{\zeta}$ is the mean mirror birefringence, $\bar{\zeta} = (\zeta_1 + \zeta_2)/2$. We assume that the signal and idler modes are close to resonance so that the corresponding round

trip phase shifts

$$\delta_{1,2} = \delta \pm \frac{\theta + \zeta_2 - \zeta_1}{2} \mp \psi \quad (4)$$

where ψ is the birefringence of the waveplate, are close to an integer multiple of 2π :

$$\delta_{1,2} = 2\pi p_{1,2} + \Delta_{1,2} \quad (5)$$

where $p_{1,2}$ are integers and $\Delta_{1,2}$ are small detunings.

In this case, the classical evolution equations given in [20] become:

$$\begin{aligned} \tau \frac{dA_1^{(s)}}{dt} &= A_1^{(s)}(-\mu' + i\Delta_1) + gA_0^{(s)}A_2^{(s)*} + i2\rho e^{i(\theta-\psi)}A_2^{(s)} \\ \tau \frac{dA_2^{(s)}}{dt} &= A_2^{(s)}(-\mu' + i\Delta_2) + gA_0^{(s)}A_1^{(s)*} + i2\rho e^{-i(\theta-\psi)}A_1^{(s)} \\ A_0^{(s)} &= A_0^{in} - \frac{g}{2}A_1^{(s)}A_2^{(s)} \end{aligned} \quad (6)$$

where A_0^{in} is the input pump amplitude at frequency ω_0 .

The stationary solution of these equations, corresponding to the phase locked regime, can be found only within a given range of detunings (Δ_1, Δ_2) which has been detailed in [20].

The evolution equations for the fluctuations then are:

$$\begin{aligned} \tau \frac{d\delta A_1}{dt} &= \delta A_1(-\mu' + i\Delta_1) \\ &\quad + g\left(A_0^{(s)}\delta A_2^* + A_2^{(s)*}\delta A_0\right) + i2\rho e^{i(\theta-\psi)}\delta A_2 \\ &\quad + \sqrt{2\kappa}\delta A_1^{in} + \sqrt{2\mu}\delta B_1^{in} \\ \tau \frac{d\delta A_2}{dt} &= \delta A_2(-\mu' + i\Delta_2) \\ &\quad + g\left(A_0^{(s)}\delta A_1^* + A_1^{(s)*}\delta A_0\right) + i2\rho e^{-i(\theta-\psi)}\delta A_1 \\ &\quad + \sqrt{2\kappa}\delta A_2^{in} + \sqrt{2\mu}\delta B_2^{in} \\ \delta A_0^{(s)} &= \delta A_0^{in} - \frac{g}{2}\left(A_2^{(s)}\delta A_1 + A_1^{(s)}\delta A_2\right) \end{aligned} \quad (7)$$

where δA_i^{in} and δB_i^{in} correspond to the vacuum fluctuations entering the cavity due respectively to the coupling mirror and to the losses. From these equations, one can calculate the Fourier components of the fluctuations and thus the spectra of variances and correlations for different quadratures of the signal and idler fields.

3 Variances

The amplitude quadrature and phase quadrature fluctuations can be written in the Fourier domain as

$$\delta \tilde{x}_i(\Omega) = \delta \tilde{A}_i(\Omega)e^{-i\varphi_i} + \delta \tilde{A}_i^*(-\Omega)e^{i\varphi_i}, \quad (8)$$

$$\delta \tilde{p}_i(\Omega) = -i\left(\delta \tilde{A}_i(\Omega)e^{-i\varphi_i} - \delta \tilde{A}_i^*(-\Omega)e^{i\varphi_i}\right), \quad (9)$$

$i = 1, 2$ where $\delta \tilde{A}_i$ denotes the Fourier component and φ_i is the phase of the stationary solution $A_i^{(s)}$.

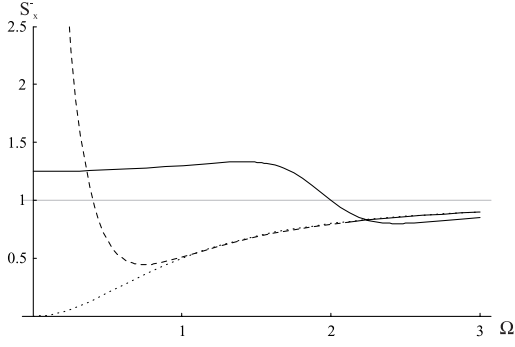


Fig. 2. Intensity difference variance spectra as a function of the normalized frequency Ω for waveplate angles $\rho = 0$ (dotted line), $\rho = 0.01$, (dashed line) and $\rho = 0.05$ (continuous line). Intracavity losses and output coupling coefficient, $(\mu, \kappa) = (0, 0.05)$. The standard quantum limit is shown in grey. These plots are independent of σ .

To characterize the entanglement, one can calculate the normalized variances of the sum and difference of the amplitude and phase quadratures [6, 21]

$$\begin{aligned} S_x^\pm(\Omega) &= \frac{1}{2} \left\langle |\delta\tilde{x}_1(\Omega) \pm \delta\tilde{x}_2(\Omega)|^2 \right\rangle \\ S_p^\pm(\Omega) &= \frac{1}{2} \left\langle |\delta\tilde{p}_1(\Omega) \pm \delta\tilde{p}_2(\Omega)|^2 \right\rangle. \end{aligned} \quad (10)$$

The fact that S_x^- and S_p^+ are smaller than one is the signature of simultaneous quantum correlations on both phase and amplitude quadratures. This is the case in a standard OPO above threshold with the restriction already mentioned in the introduction that because of the phase diffusion, S_p^+ can not be measured easily.

From the above calculated fluctuations, one can obtain the variances for any operating point. For the sake of simplicity, we consider here the case of detunings $\Delta = \pm 2\rho$ which correspond to the minimum threshold for which $\theta - \psi = \pi/2$ and $A_i^{(s)} = \sqrt{(2\mu'/g)(\sigma - 1)}e^{i\varphi_i}$, $i = 1, 2$ where σ is the input pump intensity normalized to the threshold of the standard OPO. We now have:

$$S_x^-(\Omega) = \frac{\left(\Omega^2 - \frac{4\rho^2}{\mu'^2}\right)^2 + \frac{4\rho^2}{\mu'^2} \frac{\kappa}{\mu'} + \frac{\mu}{\mu'} \Omega^2}{\left(\Omega^2 - \frac{4\rho^2}{\mu'^2}\right)^2 + \Omega^2} \quad (11)$$

$$S_p^+(\Omega) = 1 - \frac{\frac{\kappa}{\mu'}}{\Omega^2 + \sigma^2} \quad (12)$$

where $\Omega = \omega\tau/2\mu' = \omega/\Omega_c$ is the frequency normalized to the cavity cut-off frequency, Ω_c .

The expression for the phase sum variance is identical to the one obtained in the case of a standard (non phase locked) OPO: one obtains very large phase anticorrelations for any waveplate angle. The expression for the intensity difference variance is different from the expression obtained in the case of a standard OPO and does not depend on the pump power σ . The intensity difference noise reduction is now degraded at low frequencies by the phase locking: inhibition of phase diffusion prevents S_p^-

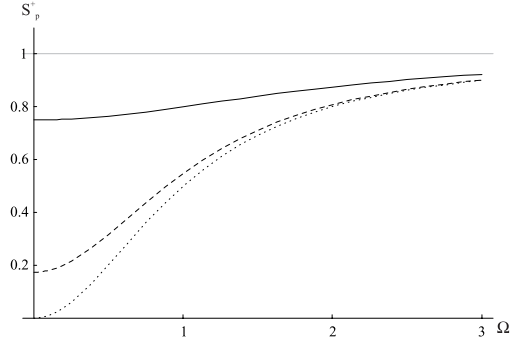


Fig. 3. Phase sum variance spectra as a function of the normalized frequency Ω for normalized pump intensity $\sigma = 1$ (dotted line), $\sigma = 1.1$ (dashed line), $\sigma = 2$ (continuous line). Intracavity losses and output coupling coefficient, $(\mu, \kappa) = (0, 0.05)$. The standard quantum limit is shown in grey. These plots do not depend on the waveplate angle ρ .

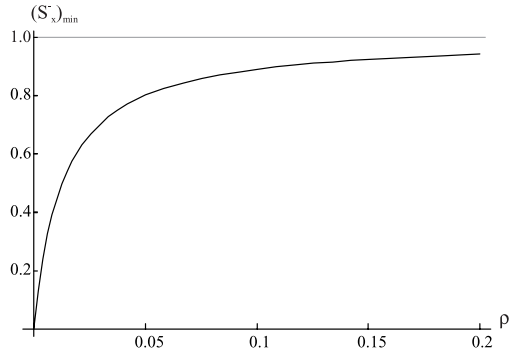


Fig. 4. $(S_x^-)_{min}$ as a function of waveplate angle ρ for intracavity losses and output coupling coefficient, $(\mu, \kappa) = (0, 0.05)$. The standard quantum limit is shown in grey.

from going to $+\infty$ as Ω goes to zero. Thus, in order to verify the corresponding Heisenberg inequality, S_p^+ cannot go to zero but instead takes a finite value.

The corresponding spectra are shown in Figures 2 and 3. These figures show that the amplitude quadrature difference variance goes to zero as ρ goes to zero while the phase quadrature sum goes to zero close to threshold.

An important characteristic of the system is the minimal value obtained for S_x^- as a function of Ω , $(S_x^-)_{min}$ which is plotted in Figure 4 as a function of ρ . This plot shows that one obtains a significant noise reduction as long as ρ is small compared to κ .

4 Entanglement criteria

4.1 EPR correlations criterion

In the *Gedanken Experiment* discussed in [4], one tries to infer the quantum state of a particle by measurements on a spatially separated particle: the optical equivalent of that scheme is to try to infer the signal beam by measurements on the spatially separated idler beam. In this case, quantum correlations do not suffice to characterize the efficiency of the system and another criterion has to be

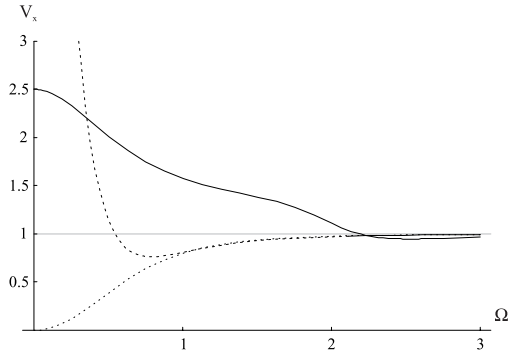


Fig. 5. Conditional variance spectra for the amplitude quadrature V_x as a function of the normalized frequency Ω for wave plate angle $\rho = 0$ (dotted line), $\rho = 0.01$, (dashed line) and $\rho = 0.05$ (continuous line). Intracavity losses and output coupling coefficient, $(\mu, \kappa) = (0, 0.05)$. The standard quantum limit is shown in grey. Normalized pump intensity $\sigma = 1$.

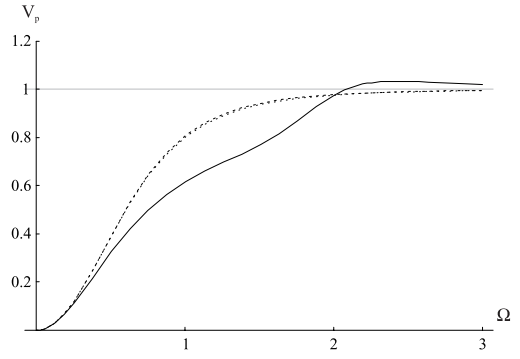


Fig. 6. Conditional variance spectra for the phase quadrature V_p as a function of the normalized frequency Ω for wave plate angle $\rho = 0$ (dotted line), $\rho = 0.01$, (dashed line) and $\rho = 0.05$ (continuous line). The first two curves cannot be distinguished on the figure. Intracavity losses and output coupling coefficient, $(\mu, \kappa) = (0, 0.05)$. The standard quantum limit is shown in grey. Normalized pump intensity $\sigma = 1$.

considered [21]. The noise on the measured observable has to be taken into account: a large noise will reduce the precision with which the unmeasured system is known. One is lead to introduce inference errors or conditional variances [21]. The conditional variances for amplitude and phase are given by:

$$V_x = \min_g \langle |\delta\tilde{x}_1 - g\delta\tilde{x}_2|^2 \rangle = \langle |\delta\tilde{x}_1 - C_x\delta\tilde{x}_2|^2 \rangle \quad (13)$$

$$V_p = \min_g \langle |\delta\tilde{p}_1 - g\delta\tilde{p}_2|^2 \rangle = \langle |\delta\tilde{p}_1 - C_p\delta\tilde{p}_2|^2 \rangle \quad (14)$$

where

$$C_x = \frac{\langle \delta\tilde{x}_1(\Omega)\delta\tilde{x}_2(-\Omega) \rangle}{\sqrt{\langle \delta\tilde{x}_1^2 \rangle \langle \delta\tilde{x}_2^2 \rangle}} \quad (15)$$

$$C_p = \frac{\langle \delta\tilde{p}_1(\Omega)\delta\tilde{p}_2(-\Omega) \rangle}{\sqrt{\langle \delta\tilde{p}_1^2 \rangle \langle \delta\tilde{p}_2^2 \rangle}} \quad (16)$$

are the normalized correlations. Reference [21] shows that one must have $V_x V_p < 1$ in order to have a demonstration of the EPR paradox.

Even with correlations factors close but not equal to unity, the conditional variances can be large if the quantum noise on the individual beams is large as is the case for the amplitude quadrature.

The conditional variances V_x and V_p are shown in Figures 5 and 6. Due to the large excess noise on the amplitude quadrature at low frequencies, V_x is large for low frequencies while V_p remains low for all frequencies. This difference between the two conditional variances is one of the main differences between our case and the other devices which have been introduced to generate bright entangled beams [5–8]: in these cases, one obtains theoretically symmetric behaviors for amplitude and phase which is not the case in our system.

The variation of $V_x V_p$ with Ω is plotted in Figure 7. This figure shows that EPR correlations exist in a broad frequency range even for large values of the waveplate angle. The behavior of the criterion is dominated by that of V_p which goes to zero as Ω goes to zero and is independent of the waveplate angle.

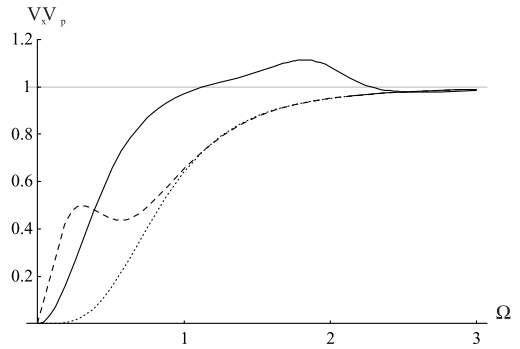


Fig. 7. $V_x V_p$ as a function of Ω for intracavity losses and output coupling coefficient, $(\mu, \kappa) = (0, 0.05)$ and for wave plate angle $\rho = 0$ (dotted line), $\rho = 0.01$, (dashed line) and $\rho = 0.05$ (continuous line). The EPR correlations limit is shown in grey. Normalized pump intensity $\sigma = 1$.

4.2 Inseparability criterion

However, this criterion is not always relevant. In the vast majority of quantum information protocols, what matters is the non-separability of the quantum state that is the impossibility to express it as a product of independent sub-states. In order to evaluate the inseparability of two systems, Peres proposed a necessary criterion which applies to finite dimension systems [22] which was latter shown by Horodecki [23] to be sufficient for dimensions smaller than 2×2 – or 2×3 –. In the particular case of Gaussian states, Duan et al. [24] and Simon [25] developed a necessary criterion for inseparability which can be written as:

$$S_x^- + S_p^+ \leq 2 \quad (17)$$

where S_x^- and S_p^+ are the previously introduced variances spectra. Let us note the entanglement produced by the self-phase locked OPO is not in the so-called standard form ([24], Eqs. (10, 11)): in this case, the above criterion is a sufficient but not necessary condition for inseparability.

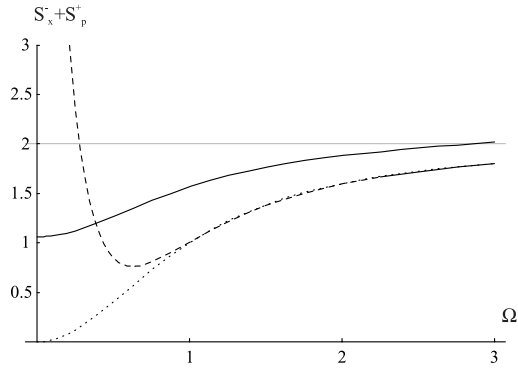


Fig. 8. $S_x^- + S_p^+$ as a function of Ω for intracavity losses and output coupling coefficient $(\mu, \kappa) = (0, 0.05)$ and wave plate angle $\rho = 0$ (dotted line), $\rho = 0.01$ (dashed line), $\rho = 0.1$ (continuous line). The inseparability limit is shown in grey.

The value of $S_x^- + S_p^+$ as a function of Ω is plotted in Figure 8. At low frequencies, the behavior is dominated by the behavior of S_x^- which is large. As higher frequencies are considered, the figure shows that the system is indeed entangled over a large range of frequencies. When $\rho \ll \kappa$, the excess noise on the amplitude quadrature makes the sum larger than two meaning that the system is separable. The curves are plotted for a value $\sigma = 1$, that is at exact threshold. Increasing σ does not increase significantly the variance S_x^- and does not modify S_p^+ and will thus move all the curves toward the inseparability limit while keeping the sum below two. It is the behavior of the amplitude fluctuations which dominates that of the sum of the variances.

4.3 Fidelity of teleportation

In teleportation experiments, one tries to transfer quantum states from one point to another with a unity gain. In this case, the successful of the teleportation is characterized by the overlap between the input and output states. This overlap is usually called the fidelity [1]. It can be shown that in order to obtain a fidelity larger than $1/2$, quantum correlations must be used, while a fidelity larger than $2/3$ denotes the possession by the receiver of the best copy available [2]. In the particular case of Gaussian states¹, one can show that the fidelity is related to the intensity difference and phase sum variances defined in equation (10) by the relation:

$$\mathcal{F} = \frac{1}{\sqrt{(1 + S_x^-)(1 + S_p^+)}}. \quad (18)$$

The fidelity as a function of the normalized frequency is shown in Figure 9 for different angles of the waveplate. One sees that for small values of the waveplate angle ρ , one obtains a fidelity larger than the “best copy” limit ($\mathcal{F} \geq 2/3$) over a large frequency range.

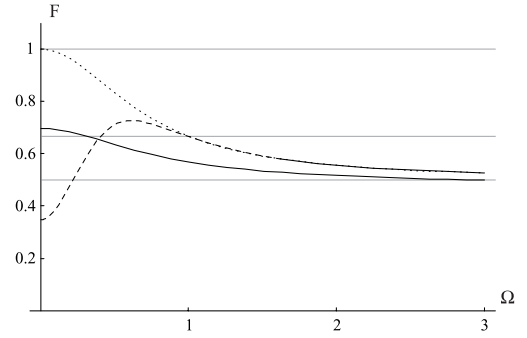


Fig. 9. Fidelity, \mathcal{F} as a function of analysis frequency Ω for intracavity losses and output coupling coefficient $(\mu, \kappa) = (0, 0.05)$ and wave plate angle $\rho = 0$ (dotted line), $\rho = 0.01$ (dashed line), $\rho = 0.1$ (continuous line). The grey lines correspond to perfect teleportation ($\mathcal{F} = 1$), “best copy” limit ($\mathcal{F} = 2/3$) and classical limit ($\mathcal{F} = 1/2$).

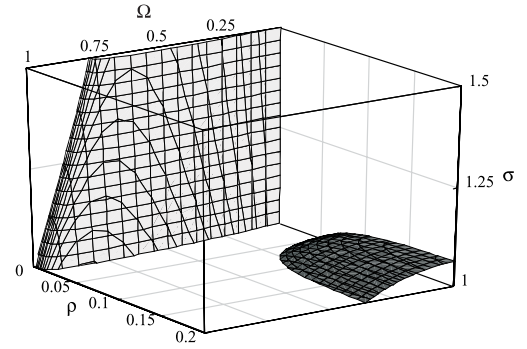


Fig. 10. Values of the analysis frequency Ω , wave plate angle ρ and normalized pump intensity σ for which $\mathcal{F} = 2/3$. Intracavity losses and output coupling coefficient $(\mu, \kappa) = (0, 0.1)$.

In order to determine the optimal operating parameters, one can plot the values of waveplate angle ρ , normalized intensity σ and analysis frequency Ω for which the fidelity is equal to the “best-copy” limit, that is $\mathcal{F} = 2/3$ (Fig. 10). The plot consists of two zones: close to threshold, i.e. $\sigma < 1.1$, one obtains a fidelity larger than $2/3$ for large values of ρ and for $\Omega < 0.5$ (dark grey surface); for $\sigma > 1.1$, a large fidelity is observed over a larger range of frequencies but only for very small values of ρ , typically $\rho < 0.02$ (light grey surface).

One observes that in order to obtain a fidelity significantly larger than $2/3$, one can use very small angles, typically less than 1° (0.015 radians). As mentioned in reference [20], this is feasible experimentally, since a small angle does not reduce the range of the crystal temperature and cavity length where the locking is observed but only its total surface: once frequency degeneracy has been obtained, existing active stabilization of the system allows for operation in this zone. However, working very close to threshold will reduce the parameter range where phase locking is observed and may be difficult experimentally.

We have shown in this section that our system produces bright entangled beams which fulfill different entanglement criteria over a large range of frequencies.

¹ And only in this case.

At low frequencies, the entanglement is observed for $\rho \ll \kappa$, that is for a rotation of the waveplate small compared to the mirror transmission.

5 Use of optimized quadratures

The limitation of the EPR correlations zone to small angle is due to the fact that the intensity correlations are no longer perfect in a phase locked OPO as was the case in the standard OPO. A simple picture shows the origin of this phenomenon. A_1 and A_2 having a fixed phase relation, the output beam is in a fixed polarization state which we denote A_{bright} . The orthogonal polarization mode has a zero mean value and is denoted A_{dark} . One can show that they correspond to the polarization eigenmodes of the “cold” OPO, that is without the pump beam [27].

One can also show that their variance spectra are

$$\begin{aligned} S_x(A_{dark}) &= \langle |\delta\tilde{x}_{dark}|^2 \rangle = \frac{1}{2} \langle |\delta\tilde{x}_1 - \delta\tilde{x}_2|^2 \rangle = S_x^- \\ S_p(A_{bright}) &= \langle |\delta\tilde{p}_{bright}|^2 \rangle = \frac{1}{2} \langle |\delta\tilde{p}_1 + \delta\tilde{p}_2|^2 \rangle = S_p^+ \end{aligned} \quad (19)$$

The exact expressions of the mean fields A_{bright} and A_{dark} depend on the choice of the operating point. For the minimum threshold point where we have performed our calculations, we have

$$A_{bright} = \frac{A_1 + A_2}{\sqrt{2}} \quad (20)$$

$$A_{dark} = \frac{A_1 - A_2}{\sqrt{2}} \quad (21)$$

which are left and right circularly polarized due to the $\pi/2$ phase shift between A_1 and A_2 .

As we have seen previously that S_x^- and S_p^+ can be smaller than the corresponding standard quantum limit, A_{bright} is phase squeezed while A_{dark} is squeezed on the orthogonal quadrature. This is shown in Figure 11 which represents the Fresnel diagram common to the fields A_1 , A_2 , A_{bright} and A_{dark} , the phase reference being the phase of the field A_{bright} .

The increase in S_x^- at low frequencies corresponds to the tilt of the corresponding squeezing ellipse (in black) with respect to the standard OPO situation (vertical ellipse in dark grey). Due to the presence of the waveplate, the amplitude quadrature of A_{dark} (measurement of the width along the horizontal axis) is not the optimal quadrature: it is thus natural to detect this optimal quadrature instead of the amplitude quadrature [28]. It is possible to dephase² appropriately A_1 with respect to A_2 so that A_{bright} and A_{dark} are now squeezed on orthogonal quadratures. In the simple case of the minimum threshold point, the new entangled are simply obtained by a linear superposition of the original fields along the neutral axis of

² For instance, by using a combination of $\lambda/2$ and $\lambda/4$ waveplates.

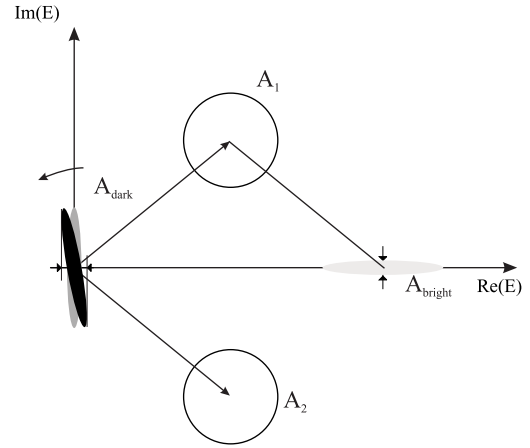


Fig. 11. Fresnel picture of the signal and idler (white surfaces), A_{bright} (light grey) and A_{dark} fields in the case of a standard OPO (black) and in the case of a phase locked OPO (dark grey).

the crystal. In the simple case of the minimum threshold point, these fields are given by:

$$A'_1 = \frac{1}{\sqrt{2}} \left[\cos\left(\frac{\theta_{opt}}{2}\right) A_1 - i \sin\left(\frac{\theta_{opt}}{2}\right) A_2 \right] \quad (22)$$

$$A'_2 = \frac{1}{\sqrt{2}} \left[\sin\left(\frac{\theta_{opt}}{2}\right) A_1 + i \cos\left(\frac{\theta_{opt}}{2}\right) A_2 \right] \quad (23)$$

where θ_{opt} is given by:

$$\theta_{opt} = \frac{1}{2} \arctan \left(\frac{2C_- \sqrt{S_x(A_{dark}) S_p(A_{dark})}}{S_x(A_{dark}) - S_p(A_{dark})} \right) \quad (24)$$

and

$$C_- = \frac{\langle \delta\tilde{x}(A_{dark}) \delta\tilde{p}(A_{dark}) \rangle}{\sqrt{S_x(A_{dark}) S_p(A_{dark})}} \quad (25)$$

The inseparability criterion developed by Duan et al. [24] is

$$S_x^+(A'_{bright}) + S_p(A'_{dark}) \leq 2 \quad (26)$$

where $S_{x,p}(A_{bright,dark})$ are defined above and $A'_{bright,dark}$ are the optimally squeezed states:

$$A'_{bright,dark} = \frac{A_1 \pm A_2}{\sqrt{2}} \quad (27)$$

Setting ρ and σ , one can plot $S_p(A'_{bright}) + S_x(A'_{dark})$ as a function of the frequency (Fig. 12). This figure shows that one can obtain a much larger violation of the inseparability criterion using optimized quadratures. For $\rho = 0.01$ rad, the value obtained is very close to the curve obtained for a standard OPO (where frequency non degeneracy and phase diffusion prevent the measurement). Furthermore, the divergence obtained at low frequencies is completely eliminated. For larger values of the waveplate angle, the improvement is still noticeable.

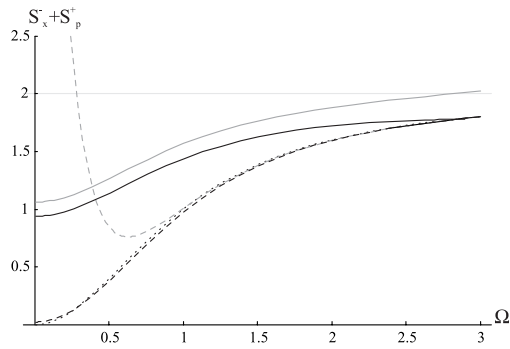


Fig. 12. $S_p (A'_{bright}) + S_x (A'_{dark})$ as a function of analysis frequency Ω for intracavity losses and output coupling coefficient $(\mu, \kappa) = (0, 0.05)$ and waveplate angle $\rho = 0$ (dotted line), $\rho = 0.01$ (dashed line), $\rho = 0.05$ (continuous line). Grey lines correspond to the curves obtained in Figure 8 for $S_p^+ + S_x^-$.

6 Conclusion

We have shown that a type II OPO containing a birefringent element can be a very efficient source of intense entangled beams. This entanglement has been characterized by the use of several criteria, namely intensity difference and phase sum variances, inference errors which denote the possibility to make an EPR-type *Gedanken Experiment*, inseparability criteria which correspond to the quality of the entanglement and fidelity which represent the quality of teleportation with unity gain. These criteria have been shown to be fulfilled for a large range of operating parameters thus showing the quality of the system. The inseparability criterion can be largely improved by the use of optimized quadratures. We are currently setting up an experiment based on this system.

Laboratoire Kastler-Brossel, of the École Normale Supérieure and the Université Pierre et Marie Curie, is associated with the Centre National de la Recherche Scientifique. This work was supported by European Community Project QUICOV IST-1999-13071. T. Coudreau is also at the Pôle Matériaux et Phénomènes Quantiques FR CNRS 2437, Université Denis Diderot, 2 place Jussieu, 75251 Paris Cedex 05, France. We thank V. Josse and N. Treps for fruitful discussions.

References

1. A. Furusawa, J.L. Sorensen, S.L. Braunstein, C.A. Fuchs, H.J. Kimble, E.S. Polzik, *Science* **282**, 706 (1998)
2. F. Grosshans, P. Grangier, *Phys. Rev. A* **64**, 010301 (2001)
3. Ch. Silberhorn, P.K. Lam, O. Weiß, F. König, N. Korolkova, G. Leuchs, *Phys. Rev. Lett.* **86**, 4267 (2001)
4. A. Einstein, B. Podolski, N. Rosen, *Phys. Rev.* **47**, 777 (1935)
5. W.P. Bowen, N. Treps, B.C. Buchler, R. Schnabel, T.C. Ralph, H. Bachor, T. Symul, P.K. Lam, *Phys. Rev. A* **67**, 032302 (2003)
6. Z.Y. Ou, S.F. Pereira, H.J. Kimble, K.C. Peng, *Phys. Rev. Lett.* **68**, 3663 (1992)
7. Y. Zhang et al., *Phys. Rev. A* **62**, 023813 (2000)
8. C. Schori, J.L. Sorensen, E.S. Polzik, *Phys. Rev. A* **66**, 033802 (2002)
9. K.C. Peng et al., *Appl. Phys. B* **66**, 755 (1998)
10. Ling-An Wu, H.J. Kimble, J.L. Hall, Huifa Wu, *Phys. Rev. Lett.* **57**, 2520 (1986)
11. J. Mertz, T. Debuisschert, A. Heidmann, Fabre, E. Giacobino, *Opt. Lett.* **16**, 1234 (1991)
12. K. Schneider, R. Bruckmeier, H. Hansen, S. Schiller, J. Mlynek, *Opt. Lett.* **21**, 1396 (1996)
13. K.S. Zhang, M. Martinelli, T. Coudreau, A. Maître, C. Fabre, *J. Opt. A: Quant. Semiclass. Opt.* **3**, 300 (2001)
14. J. Laurat, T. Coudreau, N. Treps, A. Maître, C. Fabre, *Phys. Rev. Lett.* **91**, 213601 (2003)
15. S. Reynaud, C. Fabre, E. Giacobino, *J. Opt. Soc. Am. B* **4**, 1520 (1987)
16. S. Feng, O. Pfister, *J. Opt. B: Quant. Semiclass. Opt.* **5**, 262 (2003)
17. J.-Y. Courtois, A. Smith, C. Fabre, S. Reynaud, *J. Mod. Opt.* **38**, 177 (1991)
18. E.J. Mason, N.C. Wong, *Opt. Lett.* **23**, 1733 (1998)
19. C. Fabre, E.J. Mason, N.C. Wong, *Opt. Comm.* **170**, 299 (1999)
20. L. Longchambon, J. Laurat, T. Coudreau, C. Fabre, *Eur. Phys. J. D* **30**, 279 (2004)
21. M.D Reid, *Phys. Rev. A* **40**, 913 (1989)
22. A. Peres, *Phys. Rev. Lett.* **77**, 1413 (1996)
23. P. Horodecki, *Phys. Lett. A* **232**, 333 (1997)
24. Lu-Ming Duan, G. Giedke, J.I. Cirac, P. Zoller, *Phys. Rev. Lett.* **84**, 2722 (2000)
25. R. Simon, *Phys. Rev. Lett.* **84**, 2726 (2000)
26. C. Fabre, E. Giacobino, A. Heidmann, L. Lugiato, S. Reynaud, M. VDACCHINO, Wang Kaige, *Quant. Opt.* **2**, 159 (1990)
27. L. Longchambon, J. Laurat, T. Coudreau, C. Fabre, in preparation
28. V. Josse, A. Dantan, A. Bramati, E. Giacobino, accepted in *J. Opt. B: Quant. Semiclass. Opt.* **6**(6), S532 (2004)